Measurements of proton total reaction cross sections for ^{58}Ni and ^{60}Ni including nonrelativistic and relativistic data analyses

T. Eliyakut-Roshko, R.H. McCamis,* and W.T.H. van Oers
Department of Physics, University of Manitoba, Winnipeg, Manitoba, Canada R3T 2N2

R.F. Carlson and A.J. Cox
Department of Physics, University of Redlands, Redlands, California 92373
(Received 31 May 1994)

Using a standard beam attenuation technique, proton total reaction cross sections (σ_R) for ^{58}Ni and ^{60}Ni have been measured at seven incident energies from 23 to 48 MeV to an absolute accuracy of 1 to 3%. The results have been compared both with nonrelativistic optical model predictions using global parameters and a relativistic optical model using a standard mixture of potential terms. Nuclear transparency calculations have also been made for these nuclei using all published data below 100 MeV.

PACS number(s): 25.40.Ep, 25.40.Cm, 24.10.Ht, 27.50.+e

I. INTRODUCTION

The total reaction cross section is of fundamental importance in the full understanding of a nuclear system. Values of σ_R determine, to a large extent, the imaginary potential in optical model studies of heavy nuclei [1–4]. In addition, total reaction cross sections provide significant information in few nucleon studies [5], and especially for light nuclei, provide an important constraint on phase shift analyses of elastic scattering. Recently there has been interest in measuring σ_R for light neutron-rich nuclei for the purpose of studying effects such as neutron halos [6,7]. In addition Cooper *et al.* [8] have pointed out the importance of high quality σ_R data for distinguishing among various energy-dependent global proton Dirac optical model potentials over a wide range of energies (20 to 1040 MeV).

A. Nonrelativistic models

1. Nuclear transparency calculations: Energy dependence of σ_R

It has been observed that the energy dependence of σ_R is well represented by the expression [9–12]

$$\sigma_R = \pi(R_i + \lambda)^2 \left[1 - \frac{zZe^2}{(R_i + \lambda)E}\right](1 - T) ,$$

where R_i is the effective hard-sphere interaction radius, λ is the reduced wavelength for the relative motion of the incident particle and the target nucleus, ze and E are the charge and center-of-mass kinetic energy of the incident particle, Ze is the nuclear charge, and T is the energy-dependent nuclear transparency. The quantity T can be related to the mean free path of the incident particle in the target nucleus. The two adjustable parameters are R_i and T. This equation represents a way of parametrizing σ_R data, with the transparency accounting for the difference between the maximum geometrical cross section and the smaller cross section, due to the reduced nuclear reaction probability, found at higher energies. The other free parameter R_i is given by

$$R_i = \sqrt{5/3}(r_p + r_t) ,$$

where r_p and r_t are the rms radii of the incident particle (proton) and the target nucleus, respectively. These radii are taken from tables of nucleon charge distribution parameters [13]. See Ref. [14] for a more detailed discussion plus applications to previously measured data.

2. Optical model with global parameters

The optical model used in our analysis was of standard form, containing six geometrical and five dynamical parameters. Based on the observation that the quality of the fits with fixed geometry and strength is comparable to the best fits to each individual target nucleus, the optimum proton-nucleus standard optical model parameters (the so-called global parameters) of Becchetti and Greenlees [4] were adopted here. In their work they analyzed existing elastic scattering data for incident protons of energies up to 50 MeV and scattering from nuclei of mass number between 40 and 90, and they determined an optimum general parameter set using the standard formulation of the optical model. Although the superiority of the global parameters over parameters extracted from individual analyses has not been established, it has

*Present address: AECL Research Co., Pinawa, Manitoba, Canada R0E 1L0.

been shown [3,4] that global parameters can be used with reasonable confidence.

B. Relativistic models: the relativistic optical model

An optical model based on the Dirac equation has been developed as an alternative to the Schrödinger equation based phenomenology (for example, see Refs. [8,15–30]). The basic feature of the standard relativistic optical model is its treatment of the optical potential as a mixture of a Lorentz scalar potential and the timelike component of a four-vector potential which provides the required spin-orbit and central terms. In this scalar-vector (SV) model the scalar potential is related to the neutral scalar field arising from a two-pion exchange process, and similarly, the vector potential is related to the neutral vector field composed of ω mesons. Although a model of this type has been successfully applied to the finite nuclear size and the single particle bound state problems, one can also consider other combinations which use a tensor potential to obtain the large spin-orbit strength, such as scalar-tensor (ST), VT, or SVT. The SV model has recently been applied over a wide energy range (20–400 MeV) with encouraging results [8,26,28–30], including the exhibition of systematic behavior in this energy range, which is a basic requirement for any type of phenomenological model.

II. EXPERIMENTAL METHOD

The experimental procedure consisted of a variation of a standard attenuation technique [31]. A tightly collimated, momentum-analyzed proton beam of energy known to ± 100 keV with an energy spread of ± 150 keV FWHM from the University of Manitoba sector-focused cyclotron was incident on the total reaction cross section apparatus and target, a schematic drawing of which is shown in Fig. 1. A detailed description of the apparatus and experimental technique is given in Ref. [31]. Individual protons in the incident beam were identified by signals from the two thin passing scintillation detectors 1 and 2 (in coincidence) plus the absence of signals from the two annular detectors 3 and 4. Hence the trigger signal $12\overline{(3+4)}$, the number of which is denoted as I_0,

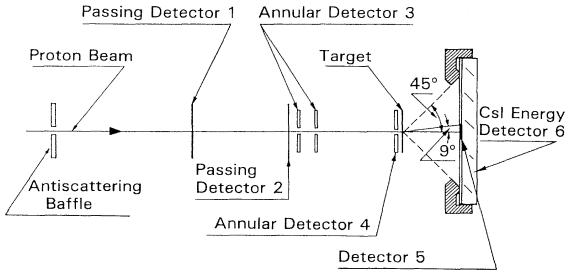

FIG. 1. Schematic diagram of the total reaction cross-section apparatus.

indicated that a properly directed proton was incident on one of the nickel targets. These targets, approximately 1 cm in diameter, were enriched to 99.79% for ^{58}Ni and 99.07% for ^{60}Ni. The areal thicknesses were 40.53 ± 0.21 mg/cm^2 for ^{58}Ni and 39.48 ± 0.14 mg/cm^2 for ^{60}Ni. Beyond the target was the stopping detector telescope, composed of the small plastic disk scintillator detector 5 and the CsI(Na) stopping detector 6. All charged particles which entered detector 5 or deposited energy in detector 6 above the ($E_{\max} - 6.0$ MeV) threshold (corresponding to elastic events plus, depending on the particular nucleus, a few inelastic states, and a small fraction of the continuum) produced an OR signal (5 + 6). The presence of an OR signal indicated a nonattenuation event I, which in most cases was an unscattered proton, but which also could have been an elastically scattered proton which entered detector 6 or a charged reaction product which entered detector 5. The OR signal I was placed in anticoincidence with the trigger signal I_0, directly yielding the difference $(I_0 - I)$, which corresponded to the number of attenuation events. The quantity $(I_0 - I)$ can be related to the total reaction cross section after applying a number of corrections which are described in Sec. III.

The experiment consisted of a series of "target in" and "target out" measurements at each of the several energies spanning the energy range 22.7 to 47.9 MeV. For each target in or target out measurement the number of attenuation events for 10^7 incident protons was measured. Each measurement was repeated two or three times, and if any of the results were more than two standard deviations from the average, that measurement was repeated. As an illustration of a sample set of data at 34.8 MeV, we measured 6202, 6223, and 6017 $(I_0 - I)$ events, each for 10^7 I_0 events for ^{58}Ni; 6100, 5986, and 6080 for ^{60}Ni, while for target out we measured 1422, 1455, 1365, 1356, 1420, 1403, and 1382 $(i_0 - i)$ events, each for 10^7 i_0 events.

III. DATA REDUCTION

The uncorrected reaction cross section σ_{un} was calculated using the formula

$$\sigma_{un} = \frac{1}{nx}\left[\frac{(I_0 - I)}{I_0} - \frac{(i_0 - i)}{i_0}\right],$$

where I_0 and i_0 are the number of trigger (incident) protons with target in and target out, respectively, $(I_0 - I)$ and $(i_0 - i)$ are the number of attenuation events with target in and target out, and nx is the number of nuclei per cm^2 in the target.

The total reaction cross section σ_R was obtained from σ_{un} after applying corrections for the following effects.

a. Elastic scattering events. Protons scattered at angles greater than 45° did not enter detectors 5 or 6, and thus were incorrectly counted as attenuation events. This correction was calculated using elastic scattering data found in the literature [3,32–39]. Even though quoted uncertainties ranged typically from 2% to 5% per data

point, we took the overall uncertainty in determining this correction, the most important of the corrections to σ_{un}, to be 10%. This correction ranged from 4.5% to 13% of the final σ_R values, and contributed less than 0.5% to the overall uncertainty in the σ_R values.

b. Charged-particle reaction products, detector 6 correction. All charged particle reaction products entering detector 6 with energies above the detector 6 threshold ($E_{\max} - 6.0$ MeV) were incorrectly counted as nonattenuation events. This correction was obtained in a manner similar to that for the elastic correction. All available inelastic differential cross section data for excited state energies up to 6 MeV for the targets under study were collected from the literature [33,34,39–42]. These cross sections were integrated over the angular range of 9°–45°, corresponding to particles missing detector 5 (0°–9°) and hitting detector 6 (0°–45°). Interpolations were made, and the corrections were determined at each of the experimental energies, which was at most 3% of the final total reaction cross section value.

c. Charged particle reaction products, detector 5 correction. All charged particles (including reaction products) entering detector 5 were counted as nonattenuation events. Since the solid angle subtended by detector 5 was small (a cone of half-angle of 9%), this correction is quite small in general, and was calculated in a way similar to that of correction (*b.*). It was always found to be about 1% of the final σ_R value.

d. Nuclear reactions occurring in detector 6. Protons which elastically scattered into detector 6 and then initiated nuclear reactions in the CsI(Na) scintillator may have been counted as attenuation events. This correction was calculated using the available data for the reaction probability for a proton stopping in CsI [43]. The number of protons entering detector 6 and missing detector 5 was counted during the experiment for the purpose of this correction. This correction was always between 3% and 4% of the final reaction cross section values.

e. Detector 5 light guide correction. Detector 5 was a scintillator disk of thickness 0.051 cm imbedded in a flat lucite light guide. A proton, elastically scattered in the lucite in such a way that it did not enter detector 6, produced a false attenuation signal. The correction for this effect was calculated using the composition of lucite and the appropriate reaction cross sections [44].

f. Other corrections. Other corrections due to target thickness and finite beam spot size were calculated and found to be negligible.

IV. RESULTS AND DISCUSSION

A. Introduction

The procedure in the nuclear transparency calculations follows that of Ref. [14]. The results will be discussed in the separate sections for each nucleus below.

For the nonrelativistic optical model analysis, we used the global parameters of Becchetti and Greenlees [4] in parametrized form in terms of A, Z, N, and E along with Schrödinger-equation-based formalism to calculate nonrelativistic σ_R values at the seven energies studied.

Relativistic optical model studies of elastic scattering using the Dirac equation with large canceling Lorentz scaler and four-vector potentials have been shown to be superior to Schrödinger-equation-based phenomenology in this energy region [27]. We have used this treatment to calculate relativistic σ_R values at several energies. The 12 potential parameters of this model (the same number of parameters as used in the nonrelativistic optical model calculation) were varied, and using the chi-square minimization method, we obtained the best fit to ^{58}Ni and ^{60}Ni differential cross section and analyzing power data found in the literature [3,32–39,45]. The analysis began with a fit to the data at 65 MeV [45]. The 65 MeV potential parameters thus obtained were then used as the starting point for analysis at lower energies, in the region of the present experiment. Reasonable fits to the data at these energies were obtained. The relativistic total reaction cross sections were then calculated using these parameters.

B. Nickel 58

The final $p + ^{58}$Ni total reaction cross section values are given in the last column of Table I, along with the associated uncertainties. The table also contains the uncorrected reaction cross sections as well as the various correction terms and all uncertainties. The largest contribution of the correction terms comes from the elastic correction, which was about 13% of σ_R at the lower energies, but which decreased with increasing energy. The total reaction cross section values are plotted as a function of incoming proton energy for ^{58}Ni in Fig. 2. Our

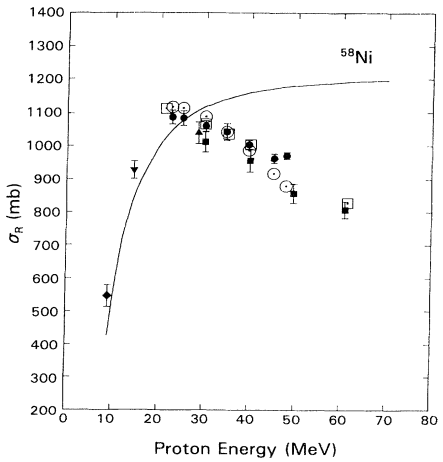

FIG. 2. Plot of σ_R (black nucleus) [Eq. (1) with $T = 0$] vs incident proton energy, as given by Table II (solid line), for ^{58}Ni. Experimental σ_R results for each nucleus are also plotted. Legend: • (this paper), ♦ (Ref. [48]), ▼ (Ref. [47]), ▲ (Ref. [32]), and ■ (Ref. [46]). Also included are Schrödinger (⊙) and Dirac (⊡) based optical model predictions for σ_R.

TABLE I. Proton total reaction cross sections for ^{58}Ni and ^{60}Ni.

Nucleus	Energy (MeV)	σ_{un} (mb)	Elastic correction (mb)	Charged particle reaction products, detector 6 correction (mb)	Charged particle reaction products, detector 5 correction (mb)	Nuclear reactions in detector 6 correction (mb)	Detector 5 light guide correction (mb)	σ_R (mb)
^{58}Ni	22.7	1221.5±13	−136.3±14	29.6±6	9.2±5	−36.7±1	−2.1±1	1085±21
	25.1	1206.2±16	−125.2±13	30.7±6	9.7±5	− 38.7±1	− 1.2±1	1082±22
	30.1	1155.5±9	−103.1±10	31.8±6	10.6±5	−36.3±1	−0.8±1	1058±16
	34.8	1117.8±21	−84.7±9	31.5±6	11.2±6	−34.0±5	−0.6±1	1041±25
	39.7	1065.4±7	−67.6±7	29.8±6	11.5±6	−35.4±1	−0.6±1	1003±13
	45.2	1008.9±11	−51.3±5	26.2±5	10.6±5	−32.2±1	−0.6±1	962±14
	47.9	1017.8±3	−44.2±4	23.8±5	11.1±6	−38.4±3	−0.6±1	970±10
^{60}Ni	22.8	1284.2±16	−114.9±12	25.5±5	8.9±5	−36.4±1	−2.1±1	1165±21
	25.1	1241.6±10	−107.7±11	27.7±6	9.5±5	−38.0±1	−1.2±1	1132±17
	30.1	1194.8±15	−92.8±9	31.4±6	10.7±5	−35.8±1	−0.8±1	1108±19
	34.8	1170.9±16	−79.7±8	33.4±7	11.9±6	−32.7±4	−0.6±1	1103±21
	39.7	1101.9±17	−67.0±7	34.0±7	12.8±6	−34.9±1	−0.6±1	1046±21
	45.2	1053.1±7	−53.8±5	32.9±6	13.4±7	−36.9±2	−0.6±1	1008±13
	47.9	1041.2±4	−47.7±5	31.7±6	13.6±7	−39.3±1	−0.6±1	999±11

TABLE II. Nuclear transparency calculation results.

Nucleus	Energy (MeV)	σ_R(exp) (mb)	Reference	σ_R (black nucleus $T = 0$) (mb)	T (%)
^{58}Ni	9.1	547±33	[48]	428	< 0
	14.5	927±27	[47]	846	< 0
	22.7	1085±21	this paper	1047	< 0
	25.1	1082±22	this paper	1076	< 0
	28.5	1038±32	[32]	1106	6.1
	30.0	1011±30	[46]	1116	9.4
	30.1	1058±16	this paper	1117	5.3
	34.8	1041±25	this paper	1141	8.8
	39.7	1003±13	this paper	1159	13.5
	40.0	955±34	[46]	1160	17.7
	45.2	962±14	this paper	1172	17.9
	47.9	970±10	this paper	1177	17.6
	49.5	856±29	[46]	1179	27.4
	60.8	807±25	[46]	1191	32.2
^{60}Ni	9.2	709±37	[48]	457	< 0
	14.5	978±16	[47]	862	< 0
	22.8	1165±21	this paper	1065	< 0
	25.1	1132±17	this paper	1093	< 0
	28.5	1053±51	[32]	1123	6.2
	30.1	1108±19	this paper	1134	2.3
	34.8	1103±21	this paper	1159	4.8
	39.7	1046±21	this paper	1176	11.1
	40.0	982±42	[46]	1177	16.6
	45.2	1008±13	this paper	1189	15.2
	47.9	999±11	this paper	1194	16.3
	60.8	841±30	[46]	1208	30.4

σ_R values are seen to vary smoothly with energy and to decrease with increasing energy. Figure 2 also contains other experimental values available from the literature [32,46–48] at 9.1, 14.5, 28.5, 30.0, 40.0, 49.5, and 60.8 MeV. In the region of energy overlap of the present work and that from the literature, our reaction cross sections are about 2% higher than those from the literature. However, within the limits of experimental uncertainties, there exists good agreement.

The results of the nuclear transparency calculations are presented in Table II. The values corresponding to a black nucleus ($T = 0$) are listed under σ_R (black nucleus) in the table and are plotted as the solid line in Fig. 2. The increasing difference between the experimental values σ_R (experimental) and σ_R (black nucleus) with increasing energy above 25 MeV is attributed to an increase (from zero) of the nuclear transparency T which is listed in column 4 of Table II. The maximum transparency of 32% occurs for the highest incident proton energy, 60.8 MeV. The calculated transparency depends on the choice of the radius parameter R_i. According to this model ^{58}Ni is completely absorbing for energies less than 25 MeV and becomes increasingly transparent to protons of energy higher than 25 MeV.

The results of the Schrödinger-equation-based optical model calculations with global parameters for $p + {}^{58}$Ni elastic data are shown in Table III. The theoretical total reaction cross section σ_R(th) values are listed in the table along with the global parameters. Values of our experimental and theoretical total reaction cross sections σ_R(exp) and σ_R(th) are plotted as a function of incident energy in Fig. 2. Although there is reasonably good agreement between experimental and theoretical reaction cross section values at energies lower than 45 MeV, it is observed that experimental results are 5% and 10% higher than optical model reaction cross section predictions at 45 and 48 MeV, respectively.

A comparison of the experimental proton total reaction cross section values for ^{58}Ni has been made with the theoretical values obtained in the Dirac-equation-based relativistic model analysis. The potential parameters of the model are listed in Table IV along with the reaction cross section predictions for ^{58}Ni. Although the real scalar and vector potential strengths decrease slightly with increasing energy while the imaginary potential strengths and shape factors remain approximately the same, a strong systematic dependence of the potential parameters on varying energy is not observed. After each parameter search, chi-square values were obtained; these are listed in Table IV. With these sets of parameters, reasonable fits to the differential cross section data were obtained at small scattering angles. The discrepancy between calculated and experimental differential cross sections at angles larger than 95° is largely due to the lack of spin observables in this low energy range for this particular nucleus. In other studies this discrepancy has been explained as a characteristic of the optical model calculations which do not include explicit exchange interactions [25]. In other studies inclusion of a complex l-dependent Majorana exchange potential in the optical model removed most of this large angle discrepancy [49,50]. A sample fit obtained from our relativistic optical model analysis of 35.2 MeV elastic data from Ref. [37] is presented in Fig. 4. The total reaction cross section predictions along with our experimental values are plotted as a function of proton energy in Fig. 2. Although there is remarkable agreement between the experimental and theoretical values, it should be pointed out that it is possible that another set of parameters may provide equally good agreement. The relativistic approach does indeed provide a testing ground for various relativistic structure calculations; however, at low energies the unambiguous specifications of the parameter set, and hence the verification of the predictions, is limited by the lack of spin data.

C. Nickel 60

The measured total reaction cross sections for $p+ {}^{60}$Ni along with the uncorrected cross sections and the associated corrections are presented in Table I. The final re-

TABLE III. Results of Schrödinger-based optical model analysis.

Nucleus	Energy (MeV)	V (MeV)	a_0 (fm)	r_0 (fm)	W_{SF} (MeV)	a_i (fm)	r_i (fm)	W_{vo} (fm)	V_{so} (MeV)	a_{so} (fm)	r_{so} (fm)	σ_R(th) (mb)	σ_R(exp) (mb)
^{58}Ni	22.73	50.44	0.75	1.17	6.52	0.53	1.32	2.30	6.20	0.75	1.01	1115	1085±21
	25.08	49.68	0.75	1.17	5.93	0.53	1.32	2.82	6.20	0.75	1.01	1112	1082±22
	30.10	48.08	0.75	1.17	4.67	0.53	1.32	3.92	6.20	0.75	1.01	1086	1058±16
	34.84	46.56	0.75	1.17	3.49	0.53	1.32	4.96	6.20	0.75	1.01	1041	1041±25
	39.77	44.98	0.75	1.17	2.26	0.53	1.32	6.05	6.20	0.75	1.01	986	1003±13
	45.13	43.27	0.75	1.17	0.92	0.53	1.32	7.23	6.20	0.75	1.01	916	962±14
	47.85	42.40	0.75	1.17	0.24	0.53	1.32	7.83	6.20	0.75	1.01	878	970±10
^{60}Ni	22.75	51.18	0.75	1.17	6.91	0.57	1.32	2.31	6.20	0.75	1.01	1172	1165±21
	25.09	50.43	0.75	1.17	6.33	0.57	1.32	2.82	6.20	0.75	1.01	1172	1132±17
	30.12	48.82	0.75	1.17	5.07	0.57	1.32	3.93	6.20	0.75	1.01	1147	1108±19
	34.86	47.31	0.75	1.17	3.89	0.57	1.32	4.97	6.20	0.75	1.01	1104	1103±21
	39.79	45.73	0.75	1.17	2.65	0.57	1.32	6.05	6.20	0.75	1.01	1049	1046±21
	45.15	44.01	0.75	1.17	1.31	0.57	1.32	7.23	6.20	0.75	1.01	979	1008±13
	47.86	43.14	0.75	1.17	0.64	0.57	1.32	7.83	6.20	0.75	1.01	941	999±11

sults have been plotted in Fig. 3; these results show a smooth variation with energy. Also included in this figure are reaction cross section results from the literature [32,46–48] for incident proton energies of 9.2, 14.5, 28.5, 40.0, and 60.8 MeV. Agreement between our results and those found in the literature is quite satisfactory.

The results of the nuclear transparency calculations are listed in Table II, with σ_R (black nucleus) and σ_R (experimental) values plotted as a function of incoming proton energy in Fig. 3. The maximum transparency of 30% occurs at 60.8 MeV, while the transparency drops to 0 at 25 MeV. According to this calculation, ^{60}Ni is almost completely absorbing for energies up to 25 MeV (just as in the case for ^{58}Ni), and then becomes increasingly transparent to incoming protons with energies higher than 25 MeV.

The results of the nonrelativistic optical model analysis with global parameters for $p + {}^{60}$Ni are shown in Table III. Our experimental total reaction cross sections for $p+{}^{60}$Ni are also plotted in Fig. 3 along with the predictions derived from the nonrelativistic optical model with global parameters. Good agreement was obtained except at 45 MeV where the experimental reaction cross section is 6% higher than the nonrelativistic optical model value.

Total reaction cross section values obtained from the relativistic optical model analysis are listed in Table IV together with the potential parameters; also in the table are chi-square values and experimental reaction cross section values for each energy. Experimental reaction cross sections for $p + {}^{60}$Ni have been plotted in Fig. 3 along with the total reaction cross section predictions from the Dirac-equation-based model. The agreement is quite remarkable. A sample fit to the differential cross section data from Ref. [37] at 35.2 MeV is presented in Fig. 4. Although the large angle discrepancy is again observed for angles greater than 90°, in a few other relativistic model analyses in the low energy range [26,28] very good agreement was obtained with large angle data, while nonrelativistic analyses require an additional term in the optical model which depends on the orbital angu-

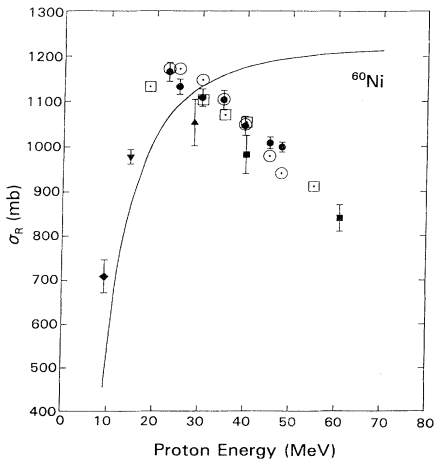

FIG. 3. Same as Fig. 2, except for ^{60}Ni.

TABLE IV. Results of Dirac-based optical model analysis.

	Energy (MeV)[a]	V_V (MeV)	R_V^1 (fm)	A_V^1 (fm)	W_V (MeV)	R_V^2 (fm)	A_V^2 (fm)	V_S (MeV)	R_S^1 (fm)	A_S^1 (fm)	W_S (MeV)	R_S^2 (fm)	A_S^2 (fm)	χ^2	σ_R(th) (mb)	σ_R(exp) (mb)	Experimental energy (MeV)[b]
^{58}Ni	21.3	223.0	1.038	0.645	−9.52	1.420	0.412	−277.0	1.079	0.691	4.18	1.025	0.411	12.0	1111		
	30.0	223.3	1.042	0.645	−9.52	1.420	0.412	−276.6	1.074	0.690	4.18	1.025	0.411	32.8	1064	1058±16	30.1
	35.2	233.3	1.041	0.645	−9.51	1.419	0.412	−276.6	1.075	0.690	4.18	1.025	0.412	42.9	1035	1041±25	34.8
	40.0	221.4	1.041	0.650	−9.52	1.430	0.411	−278.9	1.068	0.684	4.18	1.020	0.412	19.4	1003	1003±13	39.7
	61.4	262.6	1.211	0.618	−7.43	1.275	0.557	−326.6	1.209	0.631	4.41	1.110	0.438	8.2	828		
^{60}Ni	18.6	248.7	1.040	0.652	−10.82	0.421	0.412	−314.7	1.075	0.682	4.14	1.025	0.412	5.8	1132		
	30.3	249.2	1.045	0.653	−10.82	1.420	0.412	−313.9	1.068	0.681	4.14	1.025	0.412	31.5	1103	1108±19	30.1
	35.2	249.3	1.047	0.653	−10.82	1.420	0.412	−313.7	1.066	0.681	4.14	1.025	0.412	25.8	1070	1103±21	34.8
	40.0	249.3	1.047	0.653	−10.82	1.419	0.412	−313.7	1.066	0.681	4.14	1.025	0.412	20.3	1054	1046±21	39.7
	55.0	263.5	1.046	0.654	−9.49	1.412	0.411	−324.8	1.065	0.678	4.18	1.026	0.412	4.6	912		

[a]Energies at which the Dirac-based optical model calculations were performed.
[b]Energies at which the σ_R(exp) values were measured.

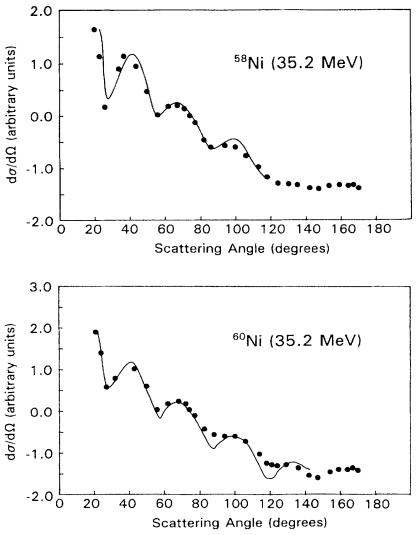

FIG. 4. Plot of Dirac based optical model fit (solid line) to 35.2 MeV proton elastic data (filled circles) from Ref. [37] for ^{58}Ni and ^{60}Ni.

lar momentum to obtain such agreement. It should also be pointed out that Cooper *et al.* [29] reported a Dirac global optical model fit for $p+$ ^{40}Ca in the energy region 21–200 MeV which resulted in somewhat lower chi-square values than ours in Table IV. However, they normalized the data so as to minimize their chi-square values.

D. Summary

In summary, we have measured total reaction cross sections for protons incident on ^{58}Ni and ^{60}Ni for seven energies between 23 and 49 MeV. Calculations of σ_R based on a nonrelativistic global optical model and the Dirac-equation-based relativistic optical model have been found to be generally in good agreement with our experimental results, with the Dirac results being closer to the experimental results than those of the nonrelativistic optical model.

ACKNOWLEDGMENTS

The authors wish to thank Dr. E. D. Cooper for his helpful suggestions regarding the relativistic data analysis. Dr. James Birchall gave us useful help in data collection and in many discussions. We are also grateful to Leslie Abernethy, Jeff Perry, Rob Poole, Tim Poole, and Alkis Rouvas for their assistance in data collection, and to Patrick Lam and Joel Peavy for their contributions to the data analysis and the preparation of this paper. This work was supported in part by the Natural Sciences and Engineering Research Council of Canada and by the Research Corporation, U.S.A.

[1] F. G. Perey, Phys. Rev. **131**, 745 (1963).
[2] P. E. Hodgson, Annu. Rev. Nucl. Sci. **17**, 1 (1967).
[3] M. P. Fricke, E. E. Gross, B. J. Morton, and A. Zucker, Phys. Rev. **156**, 1207 (1967).
[4] F. D. Becchetti and G. W. Greenlees, Phys. Rev. **182**, 1190 (1969).
[5] I. H. Sloan, Nucl. Phys. **A168**, 211 (1967).
[6] I. Tanihata, Nucl. Phys. **A488**, 113 (1988).
[7] P. G. Hansen and B. Jonson, Europhys. Lett. **4**, 409 (1987).
[8] E. D. Cooper, S. Hama, B. C. Clark, and R. L. Mercer, Phys. Rev. C **47**, 297 (1993).
[9] R. Goloskie and K. Strauch, Nucl. Phys. **29**, 474 (1962).
[10] P. U. Renberg, D. F. Measday, M. Pepin, P. Schwaller, B. Favier, and C. Richard-Serre, Nucl. Phys. **A183**, 81 (1972).
[11] R. M. DeVries and J. C. Peng, Phys. Rev. C **22**, 1055 (1980).
[12] R. E. Warner, C. P. Browne, S. E. Darden, J. J. Kolata, A. Rollefson, P. A. Kimoto, and A. Galonsky, Phys. Rev. C **37**, 1884 (1988).
[13] C. W. de Jager, H. de Vries, and C. de Vries, At. Data Nucl. Data Tables **14**, 479 (1974).
[14] R. F. Carlson, A. J. Cox, T. N. Nasr, M. S. de Jong, D. L. Ginther, D. K. Hasell, A. M. Sourkes, W. T. H. van Oers, and D. J. Margaziotis, Nucl. Phys. **A445**, 57 (1985).
[15] H. Duerr, Phys. Rev. **103**, 469 (1956).
[16] M. H. Johnson and E. Teller, Phys. Rev. **98**, 783 (1955).
[17] L. D. Miller and A. E. S. Green, Phys. Rev. C **5**, 241 (1972).
[18] R. Brockmann, Phys. Rev. C **18**, 1510 (1978).
[19] J. D. Walecka, Ann. Phys. (N.Y.) **83**, 491 (1974).
[20] S. A. Chin, Ann. Phys. (N.Y.) **108**, 301 (1977).
[21] R. L. Mercer, L. G. Arnold, and B. C. Clark, Phys. Lett. **73B**, 9 (1978).
[22] L. G. Arnold and B. C. Clark, Phys. Lett. **84B**, 46 (1979).
[23] L. G. Arnold, B. C. Clark, and R. L. Mercer, Phys. Rev. C **19**, 917 (1979).
[24] L. G. Arnold, B. C. Clark, R. L. Mercer, and P. Schwandt, Phys. Rev. C **23**, 1949 (1981).
[25] L. G. Arnold, B. C. Clark, and R. L. Mercer, Phys. Rev. C **23**, 15 (1981).
[26] B. C. Clark, S. Hama, and R. L. Mercer, in *The Interaction between Medium Energy Nucleons in Nuclei*, edited by H. O. Meyer, AIP Conf. Proc. No. 97 (AIP, New York, 1982), p. 260.
[27] B. C. Clark, invited talk presented at the Bates Users Theory Group Meeting, 1985 (unpublished).
[28] R. H. McCamis, T. N. Nasr, J. Birchall, N. E. Davison, W. T. H. van Oers, P. J. T. Verheijen, R. F. Carlson, A. J. Cox, B. C. Clark, E. D. Cooper, S. Hama, and R. L. Mercer, Phys. Rev. C **33**, 1624 (1986).
[29] E. D. Cooper, B. C. Clark, S. Hama, and R. L. Mercer, Phys. Lett. B **206**, 588 (1988).
[30] E. D. Cooper, B. C. Clark, R. Kozak, S. Shim, S. Hama,

J. I. Johansson, H. S. Sherif, R. L. Mercer, and B. D. Serot, Phys. Rev. C **36**, 2170 (1987).
[31] R. F. Carlson, W. F. McGill, T. H. Short, J. M. Cameron, J. R. Richardson, W. T. H. van Oers, J. W. Verba, P. Doherty, and D. J. Margaziotis, Nucl. Instrum. Methods **123**, 509 (1975).
[32] J. F. Turner, B. W. Ridley, P. E. Cavanagh, G. A. Gard, and A. E. Hardacre, Nucl. Phys. **58**, 509 (1964).
[33] O. N. Jarvis, B. G. Harvey, D. L. Hendrie, and J. Mahoney, Nucl. Phys. **A102**, 625 (1967).
[34] S. F. Eccles, H. F. Lutz, and V. A. Madsen, Phys. Rev. **141**, 1067 (1966).
[35] N. Baron, R. F. Leonard, and D. A. Lind, Phys. Rev. **180**, 978 (1969).
[36] H. S. Liers, R. N. Boyd, C. H. Poppe, J. A. Sievers, and D. L. Watson, Phys. Rev. C **2**, 1399 (1970).
[37] E. Fabrici, S. Micheletti, M. Pignanelli, F. G. Resmini, R. De Leo, G. D'Erasmo, and A. Pantaleo, Phys. Rev. C **21**, 844 (1980).
[38] C. B. Fulmer, J. B. Ball, A. Scott, and M. L. Whiten, Phys. Rev. **181**, 1565 (1969).
[39] M. Koike, K. Matsuda, I. Nonaka, Y. Saji, K. Yagi, H. Ejiri, Y. Ishizaki, Y. Nakajima, and E. Tanaka, J. Phys. Soc. Jpn. **21**, 2103 (1966).
[40] O. Karban *et al.*, Nucl. Phys. **A147**, 461 (1970).
[41] M. P. Fricke, E. E. Gross, and A. Zucker, Phys. Rev. **163**, 1153 (1967).
[42] D. W. Devins *et al.*, Nucl. Phys. **35**, 617 (1962).
[43] A. M. Sourkes, M. S. de Jong, C. A. Goulding, W. T. H. van Oers, E. A. Ginkel, R. F. Carlson, A. J. Cox, and D. J. Margaziotis, Nucl. Instrum. Methods **143**, 589 (1979).
[44] W. F. McGill, R. F. Carlson, T. H. Short, J. M. Cameron, J. R. Richardson, I. Slaus, W. T. H. van Oers, J. W. Verba, D. J. Margaziotis, and P. Doherty, Phys. Rev. C **10**, 2237 (1974).
[45] H. Sakaguchi, M. Nakamura, K. Hatanaka, A. Goto, T. Noro, F. Ohtani, H. Sakamoto, H. Ogawa, and S. Kobayashi, Phys. Rev. C **26**, 944 (1982).
[46] J. J. H. Menet, E. E. Gross, J. J. Malinify, and A. Zucker, Phys. Rev. C **4**, 1114 (1971).
[47] J. F. Dicello, G. J. Igo, and M. L. Roush, Phys. Rev. **157**, 1001 (1967).
[48] K. Bearpark, W. R. Graham, and G. Jones, Nucl. Phys. **73**, 206 (1965).
[49] L. G. Arnold, B. C. Clark, and R. L. Mercer, Phys. Rev. C **21**, 1899 (1980).
[50] C. J. Horowitz, Phys. Rev. C **31**, 1340 (1984).